# Bromine Nitrate Photochemistry: Quantum Yields for O, Br, and BrO Over the Wavelength Range 248−355 nm†

**R. Soller,‡,§ J. M. Nicovich,|| and P. H. Wine*,‡,||**

*School of Earth and Atmospheric Sciences and School of Chemistry and Biochemistry, Georgia Institute of Technology, Atlanta, Georgia 30332*

*Received: January 9, 2002; In Final Form: March 27, 2002*

A laser flash photolysis−resonance fluorescence technique has been employed to investigate the production of Br, O, and BrO from photodissociation of bromine nitrate ($BrONO_2$) at wavelengths in the range 248−355 nm. The values obtained for the Br atom quantum yields are $0.35 \pm 0.08$, $0.65 \pm 0.14$, $>0.62 \pm 0.11$, and $0.77 \pm 0.19$ at 248, 266, 308 and 355 nm, respectively. The values obtained for the O atom quantum yields are $0.66 \pm 0.15$, $0.18 \pm 0.04$, $<0.13 \pm 0.03$, and $<0.02$ at 248, 266, 308, and 355 nm, respectively. Quantum yields for BrO production were investigated at some of the above wavelengths by converting photolytically generated BrO to Br via the reaction $BrO + NO \rightarrow Br + NO_2$. Measured BrO quantum yields are $0.37 \pm 0.12$ at 266 nm and $0.23 \pm 0.08$ at 355 nm. Uncertainties in the above quantum yields are estimates of absolute accuracy at the 95% confidence limit. No evidence for pressure-dependent quantum yields was observed over the range 20−200 Torr in $N_2$ bath gas. No evidence for temperature-dependent quantum yields was observed either, although only a few experiments were done at temperatures other than room temperature. The above results are considered in conjunction with recently reported $NO_3$ quantum yields [Harwood; et al. *J. Phys. Chem. A* **1998**, *102*, 1309] in order to examine the role of $BrONO_2$ photochemistry in the catalytic destruction of stratospheric ozone.

## Introduction

In the stratosphere bromine nitrate ($BrONO_2$) serves both as an important reservoir species for active bromine and as an intermediate in catalytic ozone destruction cycles.[1] The formation of $BrONO_2$ occurs through the reaction of BrO with $NO_2$, and this reaction inhibits the BrO radical from depleting ozone through catalytic cycles, such as the BrO + ClO and BrO + $HO_2$ cycles.[1] Photodissociation is the most important process for converting $BrONO_2$ into catalytically "active" radicals under lower stratospheric conditions.[1] The importance of $BrONO_2$ as an intermediate in catalytic ozone-destruction cycles depends on the identity and yields of the products of photodissociation. The photolysis of $BrONO_2$ leads to the catalytic destruction of ozone only if Br and NO are produced:

$$BrONO_2 + h\nu \rightarrow Br + NO + O_2 \quad (1a)$$

$$Br + O_3 \rightarrow BrO + O_2 \quad (2)$$

$$NO + O_3 \rightarrow NO_2 + O_2 \quad (3)$$

$$\underline{BrO + NO_2 + M \rightarrow BrONO_2 + M} \quad (4)$$

$$\text{Net: } 2O_3 + h\nu \rightarrow 3O_2$$

Another variation of the above catalytic cycle results when reaction 1a proceeds through a two-step process:

$$BrONO_2 + h\nu \rightarrow Br + NO_3 \quad (1b)$$

$$\underline{NO_3 + h\nu \rightarrow NO + O_2} \quad (5)$$

$$\text{Net: } BrONO_2 + h\nu \rightarrow Br + NO + O_2 \quad (1a)$$

The yield of NO from $NO_3$ photodissociation is only 10−15%;[2−5] hence, catalytic destruction of $O_3$ is more efficient when NO is generated directly from $BrONO_2$ photolysis than when NO is generated via the combination of reactions 1b and 5. In addition to the two $BrONO_2$ photolytic pathways already mentioned (1a and 1b), several other energetically allowable channels exist at wavelengths available in the stratosphere. A complete list of all possible pathways is presented below, where the wavelengths given are the energetic thresholds for dissociation:[6]

$$BrONO_2 + h\nu \rightarrow BrO + NO_2 \quad \lambda < 1100 \text{ nm} \quad (1c)$$

$$BrONO_2 + h\nu \rightarrow Br + NO_3 \quad \lambda < 900 \text{ nm} \quad (1b)$$

$$BrONO_2 + h\nu \rightarrow Br + NO + O_2 \quad \lambda < 790 \text{ nm} \quad (1a)$$

$$BrONO_2 + h\nu \rightarrow BrONO + O \quad \lambda < 390 \text{ nm} \quad (1d)$$

$$BrONO_2 + h\nu \rightarrow Br + NO_2 + O \quad \lambda < 348 \text{ nm} \quad (1e)$$

$$BrONO_2 + h\nu \rightarrow BrO + NO + O \quad \lambda < 288 \text{ nm} \quad (1f)$$

When photolysis occurs through channels 1d−1f, a catalytic null cycle results because of the production of the oxygen atom and its subsequent reaction $O + O_2 \rightarrow O_3$; channel 1c merely reverses formation of $BrONO_2$, and as stated previously, channels 1a and 1b each participate in a catalytic destruction

† Part of the special issue "Donald Setser Festschrift".
‡ School of Earth and Atmospheric Sciences.
§ Present address: Department of Chemistry, Emory University, Atlanta, Georgia 30322.
|| School of Chemistry and Biochemistry.

10.1021/jp020018r CCC: $22.00 
Published on Web 05/01/2002

cycle. Consequently, the determination of quantum yields as a function of wavelength will assist atmospheric scientists in properly assessing the impact of $BrONO_2$ photolysis on ozone concentration levels.

Partly because $BrONO_2$ is difficult to synthesize, purify and handle, the entire literature database for $BrONO_2$ photochemistry and kinetics consists of three studies of the $BrONO_2$ absorption spectrum,[6−8] two studies of $BrONO_2$ reaction kinetics,[9,10] one study of $NO_3$ production from the $O(^3P) + BrONO_2$ reaction,[11] and one study of $NO_3$ production from the photolysis of $BrONO_2$ at 248, 308 and 352.5 nm, where the reported quantum yields are $0.28 \pm 0.09$ at 248 nm, $1.01 \pm 0.35$ at 308 nm, and $0.92 \pm 0.43$ at 352.5 nm.[9]

In the present paper, we report an experimental study of the photodissociation of $BrONO_2$ at 248, 266, 308, and 355 nm. Temperature variations were conducted for the determination of Br and BrO quantum yields at 266 nm only, and pressure variations were performed for Br, O, and BrO quantum yields at selected wavelengths. Where comparisons are appropriate, our results are reasonably consistent with the $NO_3$ quantum yields reported by Harwood et al.[9]

## Experimental Techniques

A laser flash photolysis (LFP)−resonance fluorescence (RF) technique has been employed to measure quantum yields for the photodissociation of $BrONO_2$ at 248, 266, 308, and 355 nm. Although the LFP−RF system is utilized in all experiments, two variations of the technique are necessary: one for the investigation of Br and O atom quantum yields, and the other for the investigation of BrO quantum yields. For the purpose of the present study, the two variations are referred to as the resonance fluorescence calibration technique and the BrO conversion technique, respectively.

**LFP−RF Apparatus.** This apparatus has been described in detail in previous publications from our laboratory[12,13] and, therefore, only features specific to the present study are discussed below. A schematic diagram of the current version of the apparatus is published elsewhere;[14,15] the apparatus used for this study is modified slightly (compared to the published schematic) in order to include absorption cells for the detection of $BrONO_2$.

A Pyrex jacketed reaction cell with an internal volume of $\sim$150 $cm^3$ was used in all experiments. The cell was maintained at a constant temperature by circulating ethylene glycol ($T >$ 298 K) or methanol ($T <$ 298 K) from a thermostated bath through the outer jacket. A copper−constantan thermocouple with a stainless steel jacket was inserted into the reaction zone through a vacuum seal, which allowed for the gas temperature to be measured under the precise pressure and flow rate conditions of the experiment.

Photolysis light was generated by three different lasers. A Quanta Ray Model DCR-2A Nd:YAG laser provided the light source at 355 and 266 nm, using third and fourth harmonic radiation, respectively; the pulse width was $\sim$6 ns. A KrF Lambda Physik EMG 200 excimer laser and a Lambda Physik Lextra 200 excimer laser provided the light sources at 248 and 308 nm, respectively; the pulse widths of both excimer lasers were $\sim$20 ns. The ranges of laser fluences employed in this study were as follows (in units of mJ $cm^{-2}$ $pulse^{-1}$): 2−35 at 248 nm, 4−34 at 266 nm, 3−35 at 308 nm, and 18−100 at 355 nm.

In separate experiments, the photolysis products Br and O atoms were detected directly by resonance fluorescence spectroscopy. An atomic resonance lamp, which was situated perpendicular to the photolysis laser, excited resonance fluorescence in the photolytically produced atoms. The resonance lamp consisted of an electrodeless microwave discharge, through which approximately 1 Torr of a gas mixture flowed. The gas mixture contained trace amounts of either $Br_2$ or $O_2$ in helium. Radiation passed from the lamp into the reaction cell through $MgF_2$ optics. Additionally, the region between the lamp and the reaction cell was purged with a flow of filter gases, which effectively prevented the simultaneous detection of multiple species.[12,13,16] These filter gases consisted of 50 Torr cm $CH_4$ and 60 Torr cm $O_2$ for the bromine and oxygen resonance lamps, respectively. Resonance fluorescence of atomic species in the reaction cell was focused onto the photocathode of a solar blind photomultiplier through a $MgF_2$ lens; the photomultiplier was located on an axis orthogonal to both the photolysis laser beam and the resonance lamp beam. The region between the reaction cell and the photomultiplier was purged with $N_2$ to prevent absorption of resonance fluorescence by atmospheric gases such as $O_2$ and $H_2O$. Signals were processed using photon-counting techniques in conjunction with multichannel scaling.

To avoid accumulation of photolysis products, all experiments were carried out under "slow-flow" conditions. The linear flow rate through the reactor was typically 3.5 cm $s^{-1}$ (range was 1.7−5.3 cm $s^{-1}$), and the laser repetition rate was typically 5 Hz (range was 2−10 Hz). Because photolysis occurred on an axis perpendicular to the direction of flow, no volume element of the reaction mixture was subjected to more than a few laser shots.

During experiments where Br quantum yields were studied, approximately 0.5 Torr of $CO_2$ was added to the reaction mixture in order to rapidly deactivate any photolytically generated spin−orbit excited bromine atoms, $Br(^2P_{1/2})$. The rate coefficient for electronic-to-vibrational energy transfer from $Br(^2P_{1/2})$ to ground-state $Br(^2P_{3/2})$ via collision with $CO_2$ is known to be $1.5 \times 10^{-11}$ $cm^3$ $molecule^{-1}$ $s^{-1}$.[17] This deactivation of excited-state bromine atoms avoided any problems associated with the difference in detection sensitivity for the two atomic bromine electronic states. Experiments involving the detection of oxygen atoms required no additional species in the reaction mixture. The three fine structure levels of $O(^3P_J)$ are sufficiently closely spaced in energy that it is safe to assume rapid equilibration via collisions with the $N_2$ buffer gas.

**Calibration Gases.** The system was calibrated by photolyzing known concentrations of appropriate calibrant gases. Bromine atoms were generated by the photolysis of $CF_2Br_2$ at 248 and 266 nm, a $Br_2/Cl_2$ mixture at 308 nm, and $Br_2$ at 355 nm. Oxygen atoms were generated by the photolysis of $NO_2$ at each of the four wavelengths. All investigations produced the radical of interest by photolysis, but at 308 nm an additional step was necessary because no convenient, direct photolytic source of Br atoms exists at 308 nm. Through the photolysis of the $Br_2/Cl_2$ mixture, the following mechanism provided the source of Br atoms:

$$Cl_2 + h\nu \rightarrow Cl + Cl \quad (6)$$

$$Cl + Br_2 \rightarrow Br + BrCl \quad (7)$$

Since $k_7$ is gas kinetic,[18] concentrations of $Br_2$ could readily be adjusted to make the conversion of Cl atoms to Br atoms via reaction 7 very fast compared to the rate of Br atom decay.

During Br quantum yield experiments at 308 nm, $Br_2$ was injected into the reaction cell through a $^1/_8$ in. o.d. Teflon tube positioned such that $Br_2$ mixed with other components of the gas mixture approximately 1−5 cm upstream from the reaction

zone. This method of handling $Br_2$ minimized the contact time between $Br_2$ and $Cl_2$ and prevented an unwanted source of BrCl via the dark reaction of $Br_2$ with $Cl_2$.

**Concentration Measurements.** Species concentrations in the reaction mixtures were evaluated using a combination of photometric, mass flow rate, and total pressure measurements. Photometric techniques were used to determine the concentrations of $BrONO_2$, $NO_2$, and the impurities $Br_2$ and $Br_2O$. Mass flow rate measurements were used to evaluate the concentrations of NO, $CO_2$, and the calibrants $NO_2$, $CF_2Br_2$, and $Cl_2/Br_2$. The gases $CF_2Br_2$, $Br_2$, $Cl_2$, NO, and $NO_2$ flowed into the reaction cell from separate 12-L bulbs containing dilute mixtures in nitrogen. $N_2$ and $CO_2$ were supplied directly from high-pressure tanks. The flow of $BrONO_2$ into the reaction cell was regulated by flowing nitrogen carrier gas over the $BrONO_2$ sample, which was held at temperatures in the range 220−230 K. All gases were premixed before entering the reactor, except for $Br_2$ at 308 nm (see above).

The concentration of bromine nitrate was measured both upstream and downstream of the reaction cell by UV photometry. Both absorption cells were 200 cm in length, cadmium penray lamps were used as the light source for both cells, and band-pass filters were used to isolate the cadmium line of interest. Quantitative measurements of $BrONO_2$ were made in every experiment using 228.8 nm as the monitoring wavelength; the $BrONO_2$ absorption cross section at 228.8 nm was taken to be $2.17 \times 10^{-18}$ cm$^2$.[6−8]

Absorption measurements were also made periodically at 326.1 nm (also utilizing a cadmium penray lamp emission line) in order to assess the concentration of $Br_2O$ in the reaction cell. The level of $Br_2O$ is an important parameter, since $Br_2O$ is a potentially significant source of Br, BrO, and O at 308 nm and also Br and BrO at 355 nm. Possible sources of $Br_2O$ in the reaction cell are the level of $Br_2O$ impurity in the $BrONO_2$ sample and the degree to which $Br_2O$ was generated by hydrolysis of $BrONO_2$ on the walls of the slow flow system:

$$BrONO_2 + H_2O(\text{adsorbed}) \rightarrow HOBr + HNO_3 \quad (8)$$

$$2\ HOBr \leftrightarrow Br_2O + H_2O \quad (9)$$

Due to complications that apparently involved material adsorbed onto the surface of the absorption cell windows, these concentration measurements yielded upper limits for the level of $Br_2O$ impurity (for further discussion on this topic, see ref 10). As a result, only a lower limit for the Br atom quantum yield at 308 nm and an upper limit for the O atom quantum yield at 308 nm were obtained. Although absolute quantum yield measurements at 355 nm were also affected, an additional method of analysis at 355 nm (discussed in a later section) allowed for the determination of Br and O quantum yields.

Additionally, experiments were performed to check the impurity levels of $Br_2$ and $NO_2$ in the $BrONO_2$ sample. During these experiments, the flowing gas mixture was passed through a multipass absoprtion cell that employed 457.9 nm radiation from an $Ar^+$ laser as the probe radiation. The cell had a total absorption path length of ∼3300 cm (88 passes). Both $Br_2$[19] and $NO_2$[20,21] have absorption cross sections of $\sim 5.0 \times 10^{-19}$ cm$^2$ at 457.9 nm.

**Materials.** Bromine nitrate was synthesized from the reaction of BrCl with $ClONO_2$ as first described by Spencer and Rowland,[7] $ClONO_2$ was synthesized from the reaction of $Cl_2O$ with $N_2O_5$ as first described by Schmeisser,[22] $Cl_2O$ was prepared by passing $Cl_2$(g) over solid yellow mercuric oxide as described by Cady,[23] $N_2O_5$ was prepared from the gas-phase reaction of $NO_2$ with $O_3$ as described by Ravishankara et al.,[24] and BrCl was prepared by mixing $Br_2$ with an excess of $Cl_2$ at 195 K as described by Burkholder et al.[6] The BrCl sample was purified before it was allowed to react with the $ClONO_2$ sample. This purification step consisted of a trap-to-trap distillation process, which used a series of traps held at 195, 158, and 77 K. This distillation process reduced the level of $Br_2$ impurity in $BrONO_2$, since it is easier to separate $Br_2$ from BrCl than it is to separate $Br_2$ from $BrONO_2$. Further details concerning the syntheses of $Cl_2O$, $N_2O_5$, $ClONO_2$, BrCl, and $BrONO_2$ can be found elsewhere.[14]

The gases used in this study had the following stated minimum purities: $N_2$, 99.999%; $CO_2$, 99.99%; $O_2$, 99.99%; $Cl_2$, 99.5%; $NO_2$, 99.5%. The stated purities of $Cl_2$ and $NO_2$ refer to the liquid phase in the high-pressure storage cylinder. $N_2$, $CO_2$, and $O_2$ were used as supplied, while $Cl_2$ and $NO_2$ were degassed repeatedly at 77 K before being used to prepare dilute mixtures in $N_2$ buffer gas. Ozone was prepared by passing UHP $O_2$ through a commercial ozonator. The liquid $Br_2$ sample had a stated minimum purity of 99.94%; the sample was transferred into a vial fitted with a high-vacuum stopcock and degassed repeatedly at 77 K before use.

**Resonance Fluorescence Calibration Technique.** The investigation of absolute Br and O atom quantum yields employed the resonance fluorescence calibration technique. This technique involved two integral steps: first, photolyzing a known concentration of $BrONO_2$, while monitoring the production of either Br or O atoms as a function of time by detecting the resonance fluorescence of the respective atom; and second, photolyzing a known concentration of calibrant gas with known quantum yield for producing X atoms (X = Br or O), while monitoring the production of X atoms as a function of time by the same approach. During this latter step, the detection sensitivity of the LFP−RF system was determined. The detection sensitivity is defined as the fluorescence signal per unit X atom concentration. This second step was performed both before and after the photolysis of $BrONO_2$ in order to account for any long-term drifts in detection sensitivity.

The determination of detection sensitivity requires photolyzing a known concentration of calibrant in order to produce the respective atom. A first-order decay results from the reaction of the radical with the calibrant and/or from loss by the diffusion of X atoms out of the detector's field of view. By fitting the time-dependent fluorescence signal, $S_t$, to the equation

$$\ln S_t = -k_X' t + \ln S_0 \quad (I)$$

where $k_X'$ is the pseudo-first-order rate coefficient for the decay of X atoms, the initial fluorescence signal, $S_0$, is determined. The initial X atom concentration is given by the following expression:

$$[X]_0 = [\text{calibrant}]\ \sigma_\lambda(\text{calibrant})\ \Phi_\lambda(\text{calibrant})\ F_\lambda \quad (II)$$

where $F_\lambda$ is the photolysis fluence at wavelength $\lambda$ (in units of photons area$^{-1}$ pulse$^{-1}$), $\sigma_\lambda$(calibrant) is the absorption cross section of the calibrant gas that produces X atoms at wavelength $\lambda$, and $\Phi_\lambda$(X) is the well-known quantum yield for production of X atoms from the photolysis of the calibrant gas. Comparison of detection sensitivity, $S_0/X_0$, with the initial signal level following the photolysis of $BrONO_2$, $S_0^{BN}$, yielded the concentration of photolytically generated X atoms. $S_0^{BN}$ is also determined using eq I. The absolute X atom quantum yield is calculated by using the following equations:

$$\Phi_\lambda(X) = (S_0^{BN}/[BrONO_2^*])([X]_0/S_0) \quad \text{(III)}$$

$$[BrONO_2^*] = [BrONO_2]\,\sigma_\lambda(BrONO_2)\,F_\lambda \quad \text{(IV)}$$

where $[BrONO_2^*]$ is the concentration of excited bromine nitrate molecules generated by photon absorption and $\sigma_\lambda(BrONO_2)$ is the $BrONO_2$ absorption cross section at wavelength $\lambda$.

The analysis presented above is somewhat complicated by the fact that fluorescence detection sensitivity decreases as the concentration of either the calibrant or bromine nitrate increases. This dependence of fluorescence strength on concentration is a result of two major factors: (1) the absorption of resonance radiation by both the calibrant and $BrONO_2$ along the path through the reaction cell, and (2) the collisional deactivation of excited X atoms by the calibrant and $BrONO_2$, which prevents the excited atoms from emitting fluorescent radiation. To properly account for this attenuation of fluorescence signal, the detection sensitivity, $S_0/X_0$, was measured at various calibrant concentrations, and the natural log of the detection sensitivity was plotted versus the various calibrant concentrations (see Figure 1). Next the detection sensitivity was extrapolated to zero calibrant concentration. Additionally, the analogous value for bromine nitrate, $(S_0^{BN}/[BrONO_2^*])$ from eq III, was measured at various $BrONO_2$ concentrations, plotted, and then extrapolated to zero $BrONO_2$ concentration (see Figure 2). These extrapolated values represent the limits where the fluorescence signal strength is unaffected by absorption of resonance radiation or collisional quenching of excited states. The absolute quantum yields reported in this paper are found by substituting into eq III signal levels that are corrected for attenuation of resonance fluorescence signal by $BrONO_2$ and calibrant.

**BrO Conversion Technique.** The Br to BrO quantum yield ratio, $\Phi(Br)/\Phi(BrO)$, was directly measured using this approach. Values for $\Phi(BrO)$ were determined by comparing absolute Br atom quantum yields with $\Phi(Br)/\Phi(BrO)$. During these experiments, Br was produced by adding NO to the $BrONO_2/N_2$ reaction mixture via the reaction

$$BrO + NO \rightarrow Br + NO_2. \quad (10)$$

The following mechanism was used in order to model the chemistry that followed the photolysis of a $BrONO_2/N_2/NO$ mixture:

$$Br + BrONO_2 \rightarrow Br_2 + NO_3 \quad (11)$$

$$BrO + NO \rightarrow Br + NO_2 \quad (10)$$

$$O + BrONO_2 \rightarrow BrO + NO_3 \quad (12)$$

In the above mechanism, the products of reactions 11 and 12 have yields close to unity.[9,11] Integration of the rate equations for the above mechanism (reactions 10−12) gives the equation

$$[Br] = \beta\xi(\alpha-\gamma)^{-1}\exp(-\gamma t) + \{[Br]_0 - \beta\xi(\alpha-\gamma)^{-1} - \beta([BrO]_0 - \xi)(\alpha-\beta)^{-1}\}\exp(-\alpha t) + \beta([BrO]_0 - \xi)(\alpha-\beta)^{-1}\exp(-\beta t) \quad \text{(V)}$$

In the above equation, $\alpha = k_{11}[BrONO_2]$, $\beta = k_{10}[NO]$, $\gamma = k_{12}[BrONO_2]$, and $\xi = k_{12}[BrONO_2][O]_0(\alpha-\beta)^{-1}$. Equation V was fit to the time dependent bromine atom decays in order to solve for the initial Br, BrO, and O signal levels. At photolysis wavelengths where the absolute quantum yields of Br and O were known independently from the RF calibration technique, the values of $[Br]_0$ and $[O]_0$ were fixed. The analysis then becomes a one-parameter fit for the initial BrO signal level (normalized to the Br detection sensitivity). The BrO signal level in combination with the initial Br signal level gives the quantity $\Phi(Br)/\Phi(BrO)$. A typical Br atom temporal profile measured during these experiments, as well as the best fit to eq V, is shown in Figure 3.

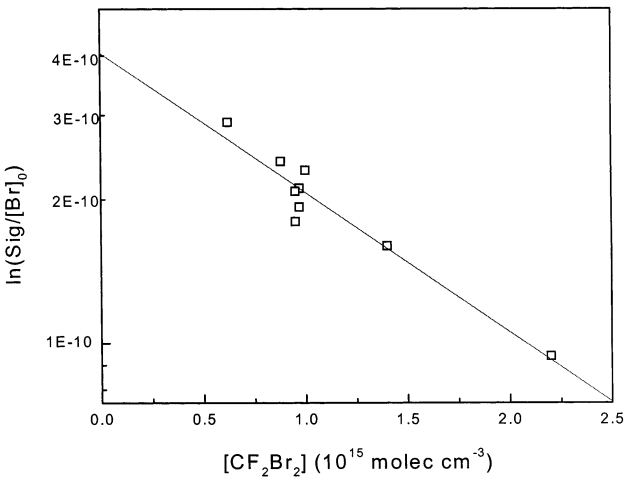


**Figure 1.** Typical plot of relative detection sensitivity versus the concentration of the calibrant $CF_2Br_2$ observed during studies of the Br atom quantum yield at 266 nm. Experimental conditions: $T = 298$ K; $P = 50$ Torr.

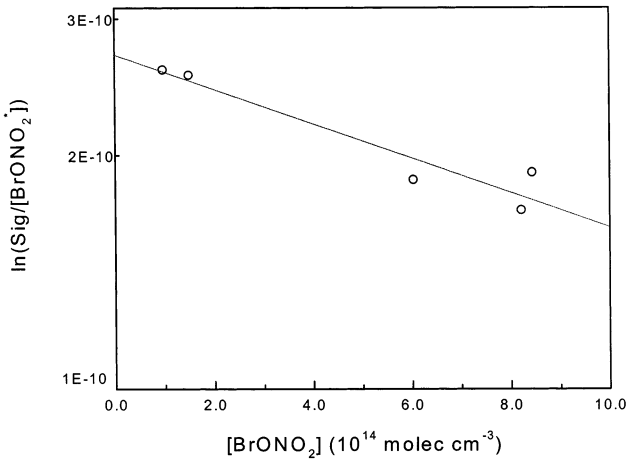


**Figure 2.** Typical plot of relative detection sensitivity versus the concentration of $[BrONO_2]$ observed during studies of the Br atom quantum yield at 266 nm. Experimental conditions: $T = 298$ K; $P = 50$ Torr.

**Additional Evaluation of Φ(Br) and Φ(BrO) at 355 nm.** This additional method of analysis allowed for the evaluation $\Phi(Br)$ and $\Phi(BrO)$ without quantitatively knowing the concentration of $Br_2O$, by using a combination of the RF calibration technique and the BrO conversion technique. This is a significant point, since $Br_2O$ produces Br and BrO upon photolysis. The $Br_2O$ absorption cross section at 355 nm is 29 times greater than that of $BrONO_2$ at the same wavelength.[6−8,25] Thus, a very small impurity of $Br_2O$ influences measurements of quantum yields for both Br and BrO.

At 355 nm, only two photolytic pathways are energetically possible for the photodissociation of $Br_2O$,

$$Br_2O + h\nu \rightarrow Br + BrO \quad \text{(13a)}$$

$$Br_2O + h\nu \rightarrow Br_2 + O \quad \text{(13b)}$$

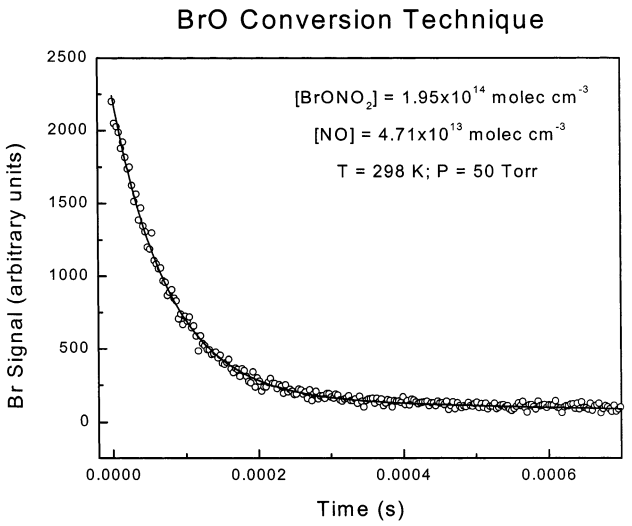


**Figure 3.** Typical resonance fluorescence temporal profile observed during a single BrO conversion technique experiment at 266 nm; number of laser shots averaged = 2000. The solid line represents a fit of the data to eq V with a single adjustable parameter (the parameter $[BrO]_0$ in eq V).

Upon examination of the above $Br_2O$ photolytic pathways, it can be inferred that $\Phi(Br) = \Phi(BrO)$, since each time an excited $Br_2O$ molecule dissociates to produce a bromine atom a molecule of bromine monoxide is also produced. This inference cannot be made at shorter wavelengths, since the photolytic pathway

$$Br_2O + h\nu \rightarrow Br + Br + O \qquad (13c)$$

becomes energetically accessible at $\lambda < 327$ nm.[26] Insufficient experimental information is available about channel 13c to allow establishment of a quantitative relationship between $\Phi(Br)$ and $\Phi(BrO)$ at shorter wavelengths. The relationship, $\Phi(Br) = \Phi(BrO)$, at 355 nm allows for the quantum yields for Br and BrO from bromine nitrate to be determined by solving a set of five linear equations. The five equations are

$$\underline{[BrONO_2^*]} = [Br]_0^{BN} + [BrO]_0^{BN} \qquad (VI)$$

$$\underline{[Br]_0} = [Br]_0^{BN} + [Br]_0^{Br_2O} \qquad (VII)$$

$$[BrO]_0 = [BrO]_0^{BN} + [BrO]_0^{Br_2O} \qquad (VIII)$$

$$[Br]_0/[BrO]_0 = \underline{Z} \qquad (IX)$$

$$[Br]_0^{Br_2O} = [BrO]_0^{Br_2O} \qquad (X)$$

In the above equations, $[Br]_0^{BN}$ and $[BrO]_0^{BN}$ are the initial concentrations of Br and BrO resulting from the photolysis of $BrONO_2$, $[Br]_0^{Br_2O}$ and $[BrO]_0^{Br_2O}$ are the initial concentrations of Br and BrO resulting from the photolysis of $Br_2O$, and $[Br]_0$ and $[BrO]_0$ are the concentrations of Br and BrO present at time zero from all known photolytic sources. In the above five equations, the five unknown values are $[Br]_0^{BN}$, $[BrO]_0^{BN}$, $[Br]_0^{Br_2O}$, $[BrO]_0^{Br_2O}$, and [BrO]. The underlined values are known from either RF calibration or BrO conversion experiments. Equation VI states that the total quantum yield for $BrONO_2$ photodissociation is unity (an assumption, but one that is almost certainly correct). Equation VII states that there is no additional source of Br atoms other than the photolysis of $BrONO_2$ and $Br_2O$. Equation VIII is analogous to eq VII for the production of BrO molecules. Equation IX defines the parameter *Z*, a quantity obtained from the BrO conversion technique. Equation X states (as discussed previously) that Br and BrO are generated simultaneously from the photolysis of $Br_2O$.

**TABLE 1: Summary of Bromine Atom Quantum Yield Data**

| Ta | $P^a$ | $[BrONO_2]^a$ | [calibrant]$^a$ | | Φ(Br) | no. of expts | $\lambda^{a,b}$ |
|---|---|---|---|---|---|---|---|
| | | | $[CF_2Br_2]$ | | | | |
| 298 | 20 | 2.37−7.77 | 0.20−1.21 | | 0.33 | 4 | 248 |
| 298 | 24 | 0.79−6.47 | 0.13−0.80 | | 0.35 | 5 | 248 |
| 298 | 123 | 1.29−4.90 | 0.23−0.75 | | 0.36 | 4 | 248 |
| | | | | | 0.35 (av) | | |
| 298 | 20 | 1.42−3.87 | 1.64−5.48 | | 0.58 | 4 | 266 |
| 298 | 50 | 1.12−7.91 | 7.29−19.5 | | 0.69 | 5 | 266 |
| 298 | 50 | 1.47−8.52 | 4.28−18.1 | | 0.66 | 9 | 266 |
| 298 | 51 | 1.12−7.39 | 4.04−19.7 | | 0.60 | 3 | 266 |
| 298 | 50 | 0.97−8.43 | 6.24−22.0 | | 0.71 | 6 | 266 |
| 298 | 48 | 1.14−8.69 | 3.58−17.3 | | 0.64 | 5 | 266 |
| 298 | 200 | 1.39−2.94 | 2.34−7.51 | | 0.62 | 3 | 266 |
| 245 | 50 | 1.90−5.21 | 2.09−6.12 | | 0.59 | 4 | 266 |
| | | | | | 0.65 (av) | | |
| | | | $[Br_2]$ | $[Cl_2]$ | 0.65 | | |
| 298 | 26 | 1.48−5.71 | 0.057−2.79 | 4.20−21.9 | >0.64 | 4 | 308 |
| 298 | 174 | 2.17−6.05 | 0.097−0.42 | 6.98−18.8 | >0.60 | 3 | 308 |
| | | | | | >0.62 (av) | | |
| 298 | 50 | 1.09−8.67 | 0.81−3.77 | | 0.79 | 6 | 355 |

$^a$ Units are *T* (K); *P* (Torr); concentrations ($10^{14}$ per $cm^3$); λ (nm). $^b$ λ ≡ photolysis laser wavelength.

**TABLE 2: Summary of Oxygen Atom Quantum Yield Data**

| $T^a$ | $P^a$ | $[BrONO_2]^a$ | $[NO_2]^a$ | Φ(O) | no. of expts. | $\lambda^{a,b}$ |
|---|---|---|---|---|---|---|
| 298 | 20 | 0.93−8.79 | 5.72−22.9 | 0.66 | 4 | 248 |
| 298 | 32 | 2.02−8.10 | 8.71−39.2 | 0.69 | 4 | 248 |
| 298 | 98 | 0.92−2.28 | 9.74−31.9 | 0.58 | 3 | 248 |
| 298 | 140 | 1.43−7.49 | 9.46−30.8 | 0.68 | 5 | 248 |
| | | | | 0.66 (av) | | |
| 298 | 20 | 5.44−10.5 | 5.16−15.1 | 0.15 | 4 | 266 |
| 298 | 19 | 2.22−8.99 | 6.07−9.93 | 0.14 | 4 | 266 |
| 298 | 20 | 2.10−5.47 | 4.52−17.8 | 0.20 | 4 | 266 |
| 298 | 50 | 2.29−5.26 | 4.03−17.8 | 0.17 | 4 | 266 |
| 298 | 51 | 1.88−4.60 | 3.98−11.9 | 0.21 | 4 | 266 |
| 298 | 100 | 2.55−7.03 | 7.52−34.2 | 0.20 | 4 | 266 |
| | | | | 0.18 (av) | | |
| 298 | 31 | 0.97−6.32 | 3.71−21.6 | 0.13 | 3 | 308 |
| 298 | 104 | 2.48−6.03 | 4.69−26.7 | 0.13 | 3 | 308 |
| | | | | 0.13 (av) | | |
| 298 | 50 | 1.53−5.28 | | <0.02 | 2 | 355 |

$^a$ Units are *T* (K); *P* (Torr); concentrations ($10^{14}$ per $cm^3$); λ (nm). $^b$ λ ≡ photolysis laser wavelength.

## Results and Discussion

All quantum yields for bromine nitrate were found to be independent of pressure. Temperature variations were performed at 266 nm for Φ(Br) and Φ(Br)/Φ(BrO), and no dependence on temperature was observed. Experimental conditions are summarized in Tables 1−3, and results are given in Table 4. All values for Φ(Br) and Φ(O) at 248, 266, and 308 nm were determined experimentally using the RF calibration technique. The reported value for Φ(Br)/Φ(BrO) at 266 nm, and thus Φ(BrO), was determined using the BrO conversion technique. Φ(Br) and Φ(BrO) were obtained at 355 nm by using both techniques and then systematically solving the set of five linear equations (see above). Quantum yields for $NO_3$ have been reported by Harwood et al.,[9] and their results are quoted in Table 4 for comparison. On the basis of examination of all possible photolytic pathways (1a)−(1f), Φ(Br) should be equal to or

**TABLE 3: Summary of Data for Φ(Br)/Φ(BrO)**

| $T^a$ | $P^a$ | $[BrONO_2]^a$ | $[NO]^a$ | Φ(Br)/Φ(BrO) | no. of expts | $\lambda^{a,b}$ |
|---|---|---|---|---|---|---|
| 298 | 20 | 1.50−2.31 | 1.29−1.94 | 1.76 | 4 | 266 |
| 298 | 49 | 1.21−3.99 | 2.84−4.45 | 1.61 | 5 | 266 |
| 298 | 50 | 1.83−3.60 | 1.16−1.48 | 1.71 | 5 | 266 |
| 298 | 50 | 2.68−2.73 | 0.82−0.91 | 1.78 | 3 | 266 |
| 298 | 50 | 1.32−5.27 | 0.48−1.48 | 1.76 | 6 | 266 |
| 298 | 52 | 0.86−4.47 | 1.14−28.7 | 1.55 | 3 | 266 |
| 298 | 200 | 1.37−3.64 | 1.45−3.05 | 2.05 | 3 | 266 |
| 245 | 50 | 2.39−4.04 | 1.10−1.32 | 1.59 | 4 | 266 |
| 323 | 50 | 1.59−3.57 | 0.89−1.01 | 1.52 | 3 | 266 |
| | | | | 1.74 (av) | | |
| 298 | 50 | 0.88−4.45 | 0.83−4.78 | 3.2 | 6 | 355 |

[a] Units are $T$ (K); $P$ (Torr); concentrations ($10^{14}$ per $cm^3$); $\lambda$ (nm). [b] $\lambda \equiv$ Photolysis laser wavelength.

**TABLE 4: Summary of Reported Bromine Nitrate Quantum Yields**

| $\lambda^a$ | $\Phi(Br)^{b,c}$ | $\Phi(O)^{b,c}$ | $\Phi(Br)/\Phi(BrO)^{b,c}$ | $\Phi(BrO)^{b,c}$ | $\Phi(NO_3)^d$ |
|---|---|---|---|---|---|
| 248 | $0.35 \pm 0.08$ | $0.66 \pm 0.15$ | | | $0.28 \pm 0.09$ |
| 266 | $0.65 \pm 0.14$ | $0.18 \pm 0.04$ | $1.74 \pm 0.43$ | $0.37 \pm 0.12$ | |
| 308 | $>0.62 \pm 0.11$ | $<0.13 \pm 0.03$ | | | $1.01 \pm 0.35$ |
| 355 | $0.77 \pm 0.19$ | $<0.02$ | $3.2 \pm 1.0$ | $0.23 \pm 0.08$ | $0.92 \pm 0.43^e$ |

[a] $\lambda \equiv$ photolysis laser wavelength in units of nm. [b] Uncertainties are $2\sigma$ and are estimates of absolute accuracy. [c] This work. [d] Reference 9. [e] 352.5 nm result.

greater than $\Phi(NO_3)$. A comparison of the two studies shows reasonable agreement. All quantum yields agree within reported uncertainties. However, further studies would be beneficial in order to improve the precision of reported quantum yields, particularly at wavelengths longer than 300 nm (where most atmospheric photolysis of $BrONO_2$ occurs).

**Quantum Yields at 355 nm.** The measured quantum yields for Br, BrO, and O are $0.77 \pm 0.19$, $0.23 \pm 0.08$, and $<0.02$, respectively. The values for Br and BrO were obtained under the assumptions that (1) the only photoloytic sources for the production of Br and BrO are $BrONO_2$ and $Br_2O$ and (2) the sum of $\Phi_{355}(Br)$ and $\Phi_{355}(BrO)$ is equal to 1. To ensure that assumption 1 is correct, all other likely sources for the photolytic production of both Br and BrO were investigated. $Br_2$ and HOBr are the only other sources of bromine atoms detected in the samples of $BrONO_2$. During selected 355 nm experiments, in situ photometric detection of $Br_2$ at 457.9 nm placed an upper limit of 3% on the $Br_2$ impurity level; the same upper limit $Br_2$ level was obtained independent of whether the multipass absorption cell was positioned upstream or downstream from the photolysis cell. Even at this upper limit, $Br_2$ would contribute only 6% to the measured value of $\Phi_{355}(Br)$, since the absorption cross sections for $Br_2$ and $BrONO_2$ are similar, $6.2 \times 10^{-20}$ [19] and $6.21 \times 10^{-20}$ $cm^2$,[6−8] respectively, and $Br_2 + h\nu \rightarrow 2Br$. HOBr was not measured during the actual LFP−RF experiments; however, UV spectroscopic analysis of the $BrONO_2$ samples placed an upper limit of 1% on the HOBr impurity level. As discussed elsewhere,[10,14] production of HOBr via $BrONO_2$ hydrolysis on the walls of the slow flow system was suppressed by pretreating the system with $N_2O_5$ (to remove adsorbed water) before each set of experiments. Based on an assumed absorption cross section for HOBr of $1.2 \times 10^{-19}$ $cm^2$ [27] and assuming a unit quantum yield for production of OH + Br,[28] we conclude that HOBr contributes a maximum of 2% to the observed Br signal. Thus it appears unlikely that either $Br_2$ or HOBr is a problem. As for other possible contributions to $\Phi_{355}(BrO)$, no other photolytic sources for BrO are known. Also, assumption (2) is almost certain to be correct because of the high $NO_3$ quantum yield measured by Harwood et al.[9] at 352.5 nm. Therefore, the 355 nm quantum yields reported in the present study are based on a total quantum yield of one. However, to further investigate assumption (2), we examined two limiting cases, which make no assumptions on the total bromine nitrate quantum yield. *Case I*: If $BrONO_2$ is the only source of Br and BrO, the total quantum yield would be the sum of the apparent Br and BrO quantum yields. *Case II*: If $Br_2O$ produced all photolytically generated BrO and thus an equal amount of Br, then the resulting Br quantum yield for $BrONO_2$ would equal the total $BrONO_2$ photodissociation quantum yield; i.e., if $\Phi(BrO) = 0$ and $\Phi_{total} = \Phi(Br) + \Phi(BrO)$, then $\Phi_{total} = \Phi(Br)$. These two limiting cases place the total bromine nitrate quantum yield in a range of 0.54−1.0. Given this range, $\Phi_{355}(Br)$ and $\Phi_{355}(BrO)$ were reevaluated. The range of values obtained for $\Phi_{355}(Br)$ and $\Phi_{355}(BrO)$ by this method of analysis are 0.54−0.79 and 0.0−0.25, respectively. Although we present these ranges of values for $\Phi_{355}(Br)$ and $\Phi_{355}(BrO)$, the reported values rely confidently on the assumption that the total photodissociation quantum yield for bromine nitrate equals 1.

**Quantum Yields at 308 nm.** The reported quantum yields for Br and O atoms are $>0.62$ and $<0.13$, respectively. Limitations in our ability to measure absolute $Br_2O$ concentrations resulted in the determination of a lower limit for Φ(Br) and an upper limit for Φ(O), since $Br_2O$ can theoretically generate both bromine and oxygen atoms upon photolysis. This limitation also prohibited measurements of Φ(BrO), since $Br_2O$ is a source of BrO.

Due (apparently) to material adsorbed onto the surface of the cell windows, only an upper limit estimate for $Br_2O$ was obtained. This estimate was obtained by assuming that all absorption measured at the monitoring wavelengths was a result of gas-phase absorption. This overestimates the level of $Br_2O$ present in the experimental system and thus overestimates the correction to Φ(Br) for bromine atoms generated from $Br_2O$. This correction decreased the measured Φ(Br) from 1.4 to $>0.62$, given that Φ(Br) from $Br_2O$ photolysis is no greater than 1.15.[29] Applying an analogous correction to Φ(O) would decrease its value below 0.13; however, Φ(O) is unknown for $Br_2O$, and therefore Φ(O) from $BrONO_2$ is quoted as an upper limit.

**Quantum Yields at 266 nm.** The measured quantum yields for Br, BrO, and O are 0.65, 0.37 and 0.18, respectively. Confidence in the data at this wavelength is strong, since the two experimental techniques for determining quantum yields are self-consistent, and interferences are minimal.

**Quantum Yields at 248 nm.** The measured quantum yield for Br atoms is 0.35, and the yield for O atoms is 0.66. These two quantum yields are confirmed by a recent study of the $NO_3$ yield from the $O(^3P) + BrONO_2$ reaction,[11] where our measured Br and O atom yields were used in a kinetic model to analyze the increase in $NO_3$ concentrations due to secondary chemistry following 248 nm laser flash photolysis of $BrONO_2$, and good agreement between model and experiment was obtained.

The measured value of $\Phi_{248}(O)$ is significantly higher than $\Phi_{266}(O)$. The yield increases from 0.18 to 0.66 over a wavelength range of only 18 nm. A change in quantum yield of this magnitude suggests either that secondary dissociation of hot $NO_3$ is much more important at 248 nm than at 266 nm or that an electronic state for $BrONO_2$ is accessible at 248 nm that is accessed weakly or not at all at 266 nm. The possibility of a new electronic state is supported by the "shoulder" in the absorption spectrum of $BrONO_2$ at ∼255 nm.[6−8] Furthermore, if the $NO_3$ quantum yield reported by Harwood et al.[9] is

considered in conjunction with the Br and O quantum yields obtained in this study, one is led to conclude that secondary dissociation of hot $NO_3$ is a minor source of O atoms. The available evidence suggests the potential importance of a BrONO + O photodissociation channel.

At 248 nm, the BrO conversion technique yielded data where the chemical mechanism (reactions 10−12) was unable to sufficiently represent the bromine temporal profiles. Thus, no quantum yield for BrO is reported at this wavelength. The observation that the chemical mechanism poorly represented the data indicates the possibility of unrecognized chemistry. Any chemistry that generates or destroys Br, O, or BrO will affect the chemical mechanism. Possible interferences include the reactions of O and Br atoms with impurities, such as $Br_2O$ and $NO_2$:

$$Br + Br_2O \rightarrow Br_2 + BrO \quad (14)$$

$$O + Br_2O \rightarrow BrO + BrO \quad (15)$$

$$O + NO_2 \rightarrow NO + O_2 \quad (16)$$

$NO_2$ was present as an impurity when NO was added to the $BrONO_2/N_2$ gas mixture. $NO_2$ was detected spectroscopically at 457.9 nm while only an $NO/N_2$ gas mixture was flowing through the system. Reaction 14 seems unlikely to be a source of error, since the mechanism properly represented the 266 nm data, where $\Phi$(Br) is nearly twice as large. However, $\Phi$(O) is significantly higher at 248 nm than at 266 nm. As a result, reactions 15 and 16 offer a possible explanation for why the mechanism properly represents 266 nm data and not 248 nm data. Although further experiments are necessary to completely understand the chemistry related to the BrO conversion technique, it is important to note that absolute quantum yields measured at 248 nm for bromine and oxygen atoms are unaffected by the possible occurrence of reactions 15 and 16.

**Error Estimates for Reported Quantum Yields.** The most important factors that contribute to the uncertainty in the quantum yields of Br, BrO, and O are as follows: $BrONO_2$ concentration measurements, laser fluence measurements, uncertainty in the quantum yields for the production of X atoms from the photolysis of the calibrant gas (for example, $\Phi$(Br) for $CF_2Br_2$ photolysis at 248 nm was taken to be $1.01 \pm 0.15$[30]), and the accuracy of measured absorption cross sections for the calibrant gases. The absolute uncertainty in the quantum yields for $BrONO_2$ are estimated from propagation of error analyses and are found to be ∼22%; this value varies slightly at each wavelength and also with the identity of the photoproduct. The actual values are given in Table 4.

One potential source of systematic error in the reported O atom quantum yields could result from secondary photolysis of BrO, $NO_2$, or $NO_3$ primary fragments. For example, BrO absorbs rather strongly in the 308−355 nm region. However, the low O atom quantum yields obtained at 308 and 355 nm rule out significant interference from secondary BrO photofragmentation. The high O atom quantum yield measured at 248 nm does not appear to be influenced by secondary photolysis effects since (a) BrO, $NO_2$, and $NO_3$ all absorb weakly at 248 nm and (b) the measured quantum yield was not affected by significant variations in photolysis laser power.

**Atmospheric Implications.** During the summer at 40° N, approximately half of the atmospheric photolysis of $BrONO_2$ occurs in the wavelength range 300−360 nm.[6] This wavelength range was investigated in the present study. The yields for channels 1a (product channel BrO + NO + $O_2$) and 1b (product channel Br + $NO_3$) are of primary interest because these channels participate in a catalytic ozone destruction cycle. The results obtained in this study in combination with those for $\Phi(NO_3)$ from Harwood et al.[9] indicate a high yield for channel 1b in the wavelength range 300−360 nm. At 308 nm the yield for this channel is greater than 0.62, and at 355 nm the yield is ∼0.8. Additionally, the possibility that channel 1a is a minor photolytic pathway in this region cannot be ruled out. Secondary dissociation to NO + $O_2$ occurs only when the primary $NO_3$ fragment has excitation energy in a narrow band between ∼16 000 $cm^{-1}$ and the energetic threshold for the $NO_2$ + O channel (17 040 ± 90 $cm^{-1}$).[31] Nonetheless, because the $BrONO_2$ catalytic cycle that includes channel 1a is considerably more efficient than the cycle that includes channel 1b, even a small yield for channel 1a is significant.

Lary[1] has reported modeling studies aimed at evaluating the relative importance of various catalytic cycles in stratospheric ozone depletion. Lary's evaluations employed the chain effectiveness, defined to be the product of the chain length and the rate of the rate-limiting step, as a measure of a catalytic cycle's importance. In the middle and upper stratosphere, catalytic cycles involving O + XO reactions as the rate-limiting steps (X = HO, NO, Cl, Br) dominate ozone destruction. However, in the lower stratosphere other bromine catalytic cycles become very important. For example, under local noon, mid-latitude, equinox conditions at $z = 20$ km, the three most effective catalytic cycles for destroying odd oxygen were evaluated by Lary[1] to be the ones with BrO + ClO, $BrONO_2$ + $h\nu$, and BrO + $HO_2$ as rate-limiting steps; chain effectiveness values for these cycles in units of molecules $cm^{-3}$ $s^{-1}$ were calculated by Lary to be approximately $1.5 \times 10^7$, $1.0 \times 10^7$, and $5 \times 10^6$, respectively. The value of $1.0 \times 10^7$ molecules $cm^{-3}$ $s^{-1}$ for the chain effectiveness of the $BrONO_2$ + $h\nu$ cycle was calculated by assuming a quantum yield of unity for channel 1b (the Br + $NO_3$ channel). If, as our results suggest, about 20% of the photodissociation proceeds via the BrO + $NO_2$ channel, then the chain effectiveness of the $BrONO_2$ cycle would be reduced by 20%. However, if the yield of channel 1a (the Br + NO + $O_2$ channel) is 0.2, a possibility that cannot be completely ruled out at this time, then the chain effectiveness of the $BrONO_2$ + $h\nu$ cycle would increase by more than a factor of 2 compared to the value calculated assuming unit yield for the Br + $NO_3$ channel. Clearly, further studies aimed at measuring absolute yields for channel 1a as a function of wavelength would be useful for further quantifying the role of $BrONO_2$ photochemistry in controlling stratospheric ozone levels.

**Acknowledgment.** This research was supported by the National Aeronautics and Space Administration−Upper Atmosphere Research Program through grants NAG5-3634 and NAG5-8931.

## References and Notes

(1) Lary, D. J. *J. Geophys. Res.* **1997**, *102*, 21515.
(2) Graham, R. A.; Johnston, H. S. *J. Phys. Chem.* **1978**, *82*, 254.
(3) Magnotta, F.; Johnston, H. S. *Geophys. Res. Lett.* **1980**, *7*, 769.
(4) Orlando, J. J.; Tyndall, G. S.; Moortgat, G. K.; Calvert, J. G. *J. Phys. Chem.* **1993**, *97*, 10996.
(5) Johnston, H. S.; Davis, H. F.; Lee, Y. T. *J. Phys. Chem.* **1996**, *100*, 4713.
(6) Burkholder, J. B.; Ravishankara, A. R.; Solomon, S. *J. Geophys. Res.* **1995**, *100*, 16793.
(7) Spencer, J. E.; Rowland, F. S. *J. Phys. Chem.* **1978**, *82*, 7.
(8) Deters, B.; Burrows, J. P.; Orphal, J. *J. Geophys. Res.* **1998**, *103*, 3563.

(9) Harwood, M. H.; Burkholder, J. B.; Ravishankara, A. R. *J. Phys. Chem. A* **1998**, *102*, 1309.
(10) Soller, R.; Nicovich, J. M.; Wine, P. H. *J. Phys. Chem. A* **2001**, *105*, 1416.
(11) Burkholder, J. B. *J. Phys. Chem. A* **2000**, *104*, 6733.
(12) Jefferson, A.; Nicovich, J. M.; Wine, P. H. *J. Phys. Chem.* **1994**, *98*, 7128 and references therein.
(13) Thorn, R. P.; Nicovich, J. M.; Cronkhite, J. M.; Wang, S.; Wine, P. H. *Int. J. Chem. Kinet.* **1995**, *27*, 369 and references therein.
(14) Soller, R. Dissertation, Georgia Institute of Technology, 1998.
(15) Finlayson-Pitts, B. J.; Pitts, J. N., Jr. *Chemistry of the Upper and Lower Atmosphere*; Academic Press: New York, 2000; p 146.
(16) Piety, C. A.; Soller, R.; Nicovich, J. M.; McKee, M. L.; Wine, P. H. *Chem. Phys.* **1998**, *231*, 155 and references therein.
(17) Peterson, A. B.; Wittig, C.; Leone, S. R. *Appl. Phys. Lett.* **1975**, *27*, 307.
(18) Nicovich, J. M.; Wine, P. H. *Int. J. Chem. Kinet.* **1990**, *22*, 379.
(19) Hubinger, S.; Nee, J. B. *J. Photochem. Photobiol. A—Chem.* **1995**, *86*, 1.
(20) Estupinan, E. G.; Nicovich, J. M.; Wine, P. H. *J. Phys. Chem. A* **2001**, *105*, 9697.
(21) Schneider, W.; Moortgat, G. K.; Tyndall, G. S.; Burrows, J. P. *J. Photochem. Photobiol. A—Chem.* **1987**, *40*, 195.
(22) Schmiesser, M. *Inorg. Synth.* **1967**, *9*, 127.
(23) Cady, G. H. *Inorg. Synth.* **1957**, *5*, 156.
(24) Ravishankara, A. R.; Wine, P. H.; Smith, C. A.; Barbone, P. E.; Torabi, A. *J. Geophys. Res.* **1986**, *91*, 5355.
(25) Orlando, J. J.; Burkholder, J. B. *J. Phys. Chem.* **1995**, *99*, 1143.
(26) Thorn, R. P.; Monks, P. S.; Stief, L. J.; Kuo, S. C.; Zhang, Z. Y.; Klemm, R. B. *J. Phys. Chem.* **1996**, *100*, 12199.
(27) Rattigan, O. V.; Lary, D. J.; Jones, R. L.; Cox, R. A. *J. Geophys. Res.* **1996**, *101*, 23021.
(28) Benter, T.; Feldmann, C.; Kirchner, U.; Schmidt, M.; Schmidt, S.; Schindler, R. N. *Ber. Bunsen-Ges. Phys. Chem.* **1995**, *99*, 1144.
(29) Burkholder, J. B. *Int. J. Chem. Kinet.* **1998**, *30*, 571.
(30) Talukdar, R. K.; Vaghjiani, G. L.; Ravishankara, A. R. *J. Chem. Phys.* **1992**, *96*, 8194.
(31) Davis, H. F.; Ionov, P. I.; Ionov, S. I.; Wittig, C. *Chem. Phys. Lett.* **1993**, *215*, 214.